HP1-β is required for development of the cerebral neocortex and neuromuscular junctions

Rebecca Aucott,[2] Jörn Bullwinkel,[1] Yang Yu,[3] Wei Shi,[3] Mustafa Billur,[1] Jeremy P. Brown,[2] Ursula Menzel,[4] Dimitris Kioussis,[4] Guozheng Wang,[5] Ingrid Reisert,[6] Jörg Weimer,[7] Raj K. Pandita,[8] Girdhar G. Sharma,[8] Tej K. Pandita,[8] Reinald Fundele,[3] and Prim B. Singh[1,2]

[1]Division of Immunoepigenetics, Department of Immunology and Cell Biology, Research Center Borstel, D-23845 Borstel, Germany
[2]Division of Genetics and Genomics, Roslin Institute, University of Edinburgh, Midlothian EH25 9PS, Scotland, UK
[3]Department of Development and Genetics, Uppsala University, S-75236 Uppsala, Sweden
[4]Division of Molecular Immunology, National Institute of Medical Research, London NW7 1AA, England, UK
[5]School of Biological Sciences, University of Liverpool, Liverpool L69 7ZB, England, UK
[6]Department of Anatomy and Cell Biology, University of Ulm, D-89069 Ulm, Germany
[7]Clinic of Obstetrics and Gynecology, Laboratory of Oncology, University Hospital Schleswig-Holstein, D-24105 Kiel, Germany
[8]Department of Radiation Oncology, Washington University School of Medicine, St. Louis, MO 63108

HP1 proteins are thought to be modulators of chromatin organization in all mammals, yet their exact physiological function remains unknown. In a first attempt to elucidate the function of these proteins in vivo, we disrupted the murine *Cbx1* gene, which encodes the HP1-β isotype, and show that the *Cbx1*$^{-/-}$-null mutation leads to perinatal lethality. The newborn mice succumbed to acute respiratory failure, whose likely cause is the defective development of neuromuscular junctions within the endplate of the diaphragm. We also observe aberrant cerebral cortex development in *Cbx1*$^{-/-}$ mutant brains, which have reduced proliferation of neuronal precursors, widespread cell death, and edema. In vitro cultures of neurospheres from *Cbx1*$^{-/-}$ mutant brains reveal a dramatic genomic instability. Our results demonstrate that HP1 proteins are not functionally redundant and that they are likely to regulate lineage-specific changes in heterochromatin organization.

Introduction

In mammals, there are three homologues of *Drosophila melanogaster* HP1, termed HP1-α, HP1-β, and HP1-γ (Jones et al., 2000). They share a high degree of sequence similarity and localize, to a lesser or greater extent, to constitutive heterochromatin: HP1-α and HP1-β are usually found enriched at sites of constitutive heterochromatin, whereas HP1-γ has a more uniform distribution (Dialynas et al., 2007). All three proteins are comprised of an N-terminal chromodomain (CD), an intervening "hinge" region, and a C-terminal chromoshadow domain (CSD) that dimerizes to form a hydrophobic pocket that can accommodate a pentapeptide sequence, PxVxL, found in several HP1-interacting partners (Thiru et al., 2004). Of the three proteins, HP1-β is the most studied.

HP1-β localizes to constitutive heterochromatin through a variety of interactions with chromatin. One involves a dynamic interaction (association constant in the micromolar range) of the HP1-β CD with Me(3)K9H3 that results from the enzymatic activities of KMT1A/B (Rea et al., 2000; Cheutin et al., 2003; Festenstein et al., 2003). In cells taken from double-null *KMT1A/B* mutant mice, which are viable albeit runted (Peters et al., 2001), the enrichment of both Me(3)K9H3 and Me(3)K20H4 at centromeric heterochromatin is lost, and HP1 proteins appear homogeneously distributed throughout both the eu- and heterochromatin (Kourmouli et al., 2004, 2005; Schotta et al., 2004). Structural

R. Aucott, J. Bullwinkel, and Y. Yu contributed equally to this paper.

Correspondence to Prim B. Singh: psingh@fz-borstel.de

R. Aucott's present address is Medical Research Council Centre for Inflammation Research, Queen's Medical Research Institute, University of Edinburgh, Edinburgh EH16 4TJ, Scotland, UK.

J.P. Brown's present address is Children's Hospital Oakland Research Institute, Oakland, CA 94609.

Abbreviations used in this paper: AChR, acetylcholine receptor; CD, chromodomain; CP, cortical plate; CSD, chromoshadow domain; df, degree of freedom; DP, double positive; LCR, locus control region; MEF, murine embryonic fibroblast; NeuN, neuronal nuclei; NF, neurofilament; PCD, premature centromere division; PEV, position-effect variegation; PNA, peptide nucleic acid; SP, subplate; VZ, ventricular zone.

The online version of this article contains supplemental material.

© 2008 Aucott et al. This article is distributed under the terms of an Attribution–Noncommercial–Share Alike–No Mirror Sites license for the first six months after the publication date (see http://www.jcb.org/misc/terms.shtml). After six months it is available under a Creative Commons License (Attribution–Noncommercial–Share Alike 3.0 Unported license, as described at http://creativecommons.org/licenses/by-nc-sa/3.0/).

The Rockefeller University Press $30.00
J. Cell Biol. Vol. 183 No. 4 597–606
www.jcb.org/cgi/doi/10.1083/jcb.200804041

THE JOURNAL OF CELL BIOLOGY

Downloaded from http://rupress.org/jcb/article-pdf/183/4/597/1554702/jcb_200804041.pdf by guest on 09 February 2026

analysis of the HP1-β CD–Me(3)K9H3 interaction reveals that the histone tail inserts as a β strand, completing the β-sandwich architecture of the HP1-β CD (Nielsen et al., 2001). The binding of HP1-β to Me(3)K9H3 is part of an epigenetic pathway in mammals: HP1-β bound to Me(3)K9H3 acts as an adapter to recruit KMT5B/C methyltransferases that trimethylate lysine 20 on histone H4 (Kourmouli et al., 2004, 2005; Schotta et al., 2004). The pathway from Me(3)K9H3 to Me(3)K20H4 via HP1 is thought to be important for the assembly of HP1-containing constitutive heterochromatin (Kourmouli et al., 2004, 2005; Schotta et al., 2004). A second mode of interaction is the binding of the HP1-β CD with the histone fold domain of histone H3 (Nielsen et al., 2001). This binding is of high affinity (in the nanomolar range; resistant to 0.6 M of salt) and is thought to represent the immobile HP1-β fraction (∼5%) in heterochromatin observed in FRAP experiments (Nielsen et al., 2001; Schmiedeberg et al., 2004; Dialynas et al., 2006). An interaction of HP1-β with methylated K26 histone H1.4 has also been shown (Daujat et al., 2005), although its significance is not known.

As part of constitutive heterochromatin, HP1 homologues are found at both the centromeres and telomeres of nearly all eukaryotic chromosomes, and the proper maintenance of these chromosomal regions is critical for genome integrity (Fanti and Pimpinelli, 2008). Mammalian HP1 proteins found at pericentric heterochromatin have been implicated in recruiting both the cohesin complex and kinetochore proteins that are necessary for chromosome segregation at mitosis and the avoidance of aneuploidy (Nonaka et al., 2001; Zhang et al., 2007). The overexpression of HP1-β in human cells results in reduced association of human telomerase reverse transcriptase with the telomere and a higher frequency of end to end chromosomal fusions, indicating that the concentration of HP1-β in the nucleus can affect telomere function (Sharma et al., 2003).

In this study, we show that the mammalian *Cbx1* gene, which encodes HP1-β, is essential for viability; thus, the HP1 isoforms are not functionally redundant. The loss of HP1-β protein leads to defective neuromuscular and cerebral cortex development. The defect in the latter is likely to be the result of a dramatic increase in genomic instability.

Results and discussion

We disrupted the *Cbx1* gene using standard techniques (Fig. 1, A–C). Crosses between $Cbx1^{+/-}$ heterozygotes, which were indistinguishable from wild-type littermates, revealed that embryonic day 19 (E19) $Cbx1^{-/-}$ embryos were significantly smaller than their $Cbx1^{+/-}$ and wild-type littermates (Fig. 1 C). The $Cbx1^{-/-}$ homozygotes died at, or a few hours after, birth. HP1-β was not detected in $Cbx1^{-/-}$ nuclear extracts using specific antibodies to either the N or C terminus of HP1-β (see Fig. 3 I and Fig. S1, available at http://www.jcb.org/cgi/content/full/jcb.200804041/DC1). For initial characterization, we tested whether the *Cbx1* mutation was a modifier of position-effect variegation (PEV) by introducing the mutation into mice heterozygous for the hCD2-1.3B variegating transgene located within centromeric constitutive heterochromatin (Festenstein et al., 1999). As shown in Fig. 1 D, there is a highly significant difference between hCD2 expression in the $Cbx1^{-/-}$ animals and the parental genotypes ($P < 0.001$). The difference between $Cbx1^{+/-}$ and $Cbx1^{+/+}$ is not significant. These data confirm that HP1-β can regulate heterochromatin-mediated gene silencing in vivo but that the sensitivity of hCD2 expression to *Cbx1* gene dosage is coarse because only when both copies of *Cbx1* are mutated is there a significant reduction in hCD2 repression (Fig. 1 D).

The coarse sensitivity of hCD2 variegation to *Cbx1* gene dosage contrasts with the situation in *Drosophila*, in which loss of a single copy of the *HP1* gene by introduction of the *Suvar205* mutation into flies that variegate for *white* significantly reduces repression (Eissenberg et al., 1990). This apparent species-specific difference in the sensitivity of PEV to gene dosage might be explained by the so-called mass action model of PEV (Locke et al., 1988). In this model, changes in the dosage of genes whose products are incorporated as tetramers (or higher order oligomers) have a much greater effect on heterochromatin formation (and thus repression) than genes whose products are incorporated monomers or dimers into heterochromatin. Given the coarse sensitivity of hCD2 variegation to *Cbx1* gene dosage (Fig. 1 D), we suggest that HP1-β is incorporated into the mammalian heterochromatin in a dimeric form. This would be consistent with structural evidence, which shows that HP1-β forms stable dimers through CSD–CSD interactions (Thiru et al., 2004), and with a kinetic model based on FRAP analysis, which indicates that swi6p (the fission yeast HP1) is incorporated into yeast heterochromatin through one-to-one homotypic interactions (Cheutin et al., 2004). The fine sensitivity of *Drosophila white* variegation to *HP1* gene dosage (Eissenberg et al., 1990) might reflect incorporation of the *Drosophila* HP1 protein into heterochromatin as higher order oligomers. Thus, although certain structural components of heterochromatin (proteins or RNAi) may be conserved across species, their stoichiometry during heterochromatin formation might be species dependent.

$Cbx1^{-/-}$ neonates exhibited no gross morphological abnormalities in the major organs. However, we observed that the lung alveoli remained collapsed after birth, indicating that perinatal death was a result of respiratory failure (Fig. 2 A). This suggested a defect in neuromuscular function. Whole mount staining of E19 diaphragms (Fig. 2 B) using antibodies to neurofilament (NF) to stain axons and α-bungarotoxin to stain postsynaptic acetylcholine receptors (AChRs) revealed that axonal growth is unaffected in $Cbx1^{-/-}$ animals, although there is sometimes a reduction in the amount of branching (Fig. 2 B, bottom). However, in $Cbx1^{-/-}$ diaphragms, we observed a significant reduction in the number of AChR clusters per micrometer of nerve ($P < 0.004$; Table S1, available at http://www.jcb.org/cgi/content/full/jcb.200804041/DC1), indicating that the likely proximate cause of death is the inability of the diaphragm to respond to the activating signals from the intramuscular nerve. The staining of thigh muscle revealed a similar decrease in AChR clustering ($P < 0.001$; Table S1), indicating that the $Cbx1^{-/-}$ mutation has a widespread effect on neuromuscular development in mutant embryos.

The defect in neuromuscular development prompted us to examine other neuronal structures, such as the developing cerebral cortex in wild-type and $Cbx1^{-/-}$ embryos. The staining of developing neocortices at days E17 (Fig. 3, A, B, E, and F) and E19 (Fig. 3, C, D, G, and H) with a marker of postmitotic neurons,

Downloaded from http://rupress.org/jcb/article-pdf/183/4/597/1554702/jcb_200804041.pdf by guest on 09 February 2026

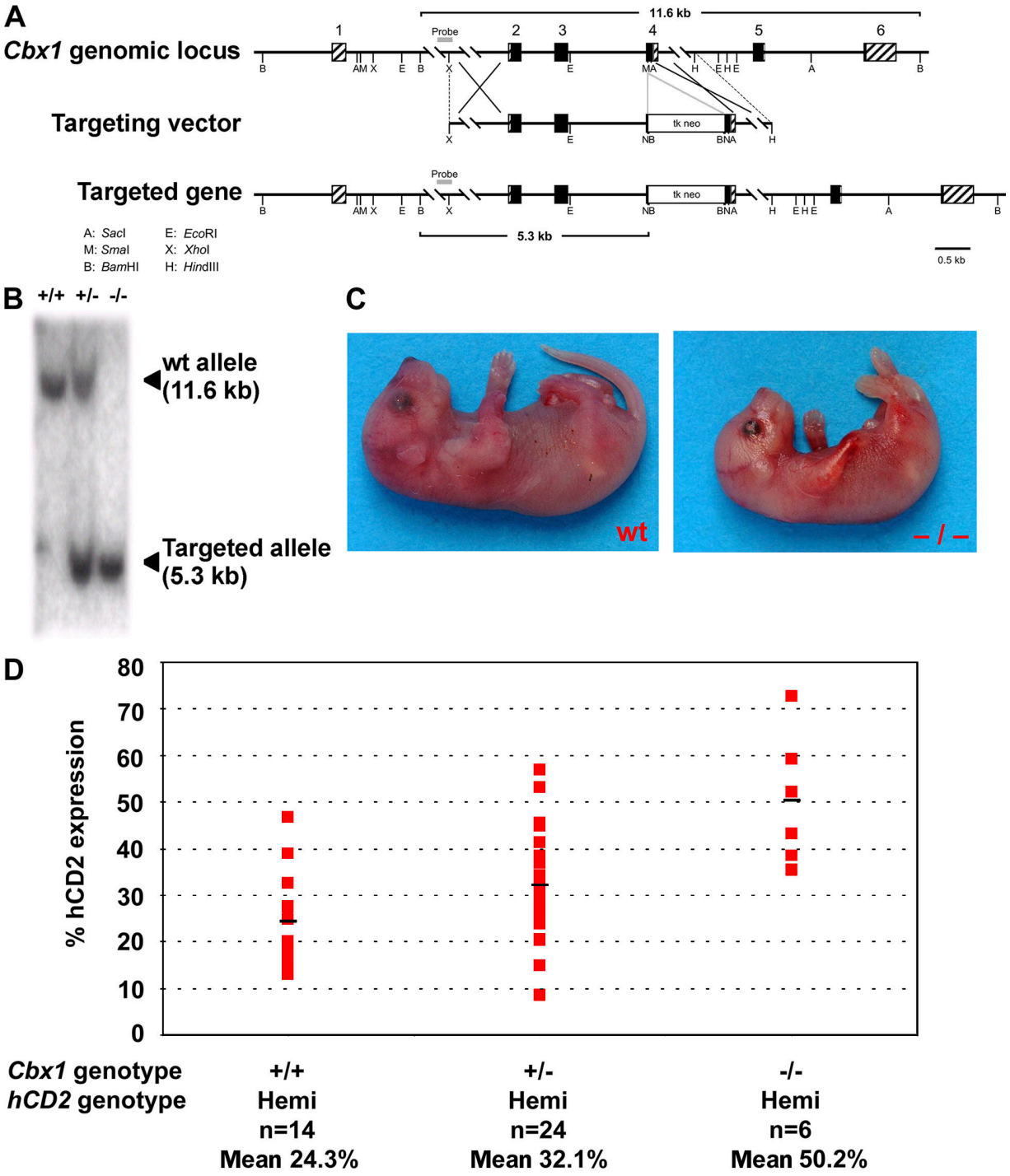

Figure 1. ***Cbx1* gene function is essential, and its product, HP1-β, is a modifier of PEV.** (A) The relevant regions in the wild-type *Cbx1* locus (top; see Materials and methods), the TK-*Neo*^{r} targeting vector (middle), and the targeted gene (bottom). Coding regions are depicted by closed boxes. Noncoding regions are denoted by striped boxes. The DNA probe used to screen for targeting events is shown as a shaded rectangle. (B) Southern blot authentication of germline transmission of the *Cbx1* mutation. BamHI digest of genomic DNA produces an 11.6-kb fragment for the wild-type (wt) allele and a diagnostic 5.3-kb fragment for the targeted allele. (C) Images of wild-type (left) and $Cbx1^{-/-}$ (right) neonates. (D) Scatter plots showing the results of flow cytometry analysis of the proportion of transgenic embryonic DP ($CD4^+CD8^+$) thymocytes that express hCD2 taken from the three *Cbx1* genotypes. Each point represents the result from a single embryo. The mean expression of hCD2 in embryonic thymocytes from $Cbx1^{+/-}$ animals is higher than that for $Cbx1^{+/+}$ animals, but not significantly. The mean expression of hCD2 in thymocytes taken from $Cbx1^{-/-}$ animals is significantly different from expression in thymocytes taken from the parental genotypes ($P < 0.001$). Black lines represent the means.

neuronal nuclei (NeuN), showed clear differences between wild-type and $Cbx1^{-/-}$ neocortices. Specifically, we observed that subplate (SP) neurons of the E17 wild-type neocortex were stained with NeuN and formed a distinct boundary between the cortical plate (CP) and the intermediate zone, but in E17 $Cbx1^{-/-}$ brains, SP neurons were very weakly stained (Fig. 3, compare E with F).

Downloaded from http://rupress.org/jcb/article-pdf/183/4/597/1554702/jcb_200804041.pdf by guest on 09 February 2026

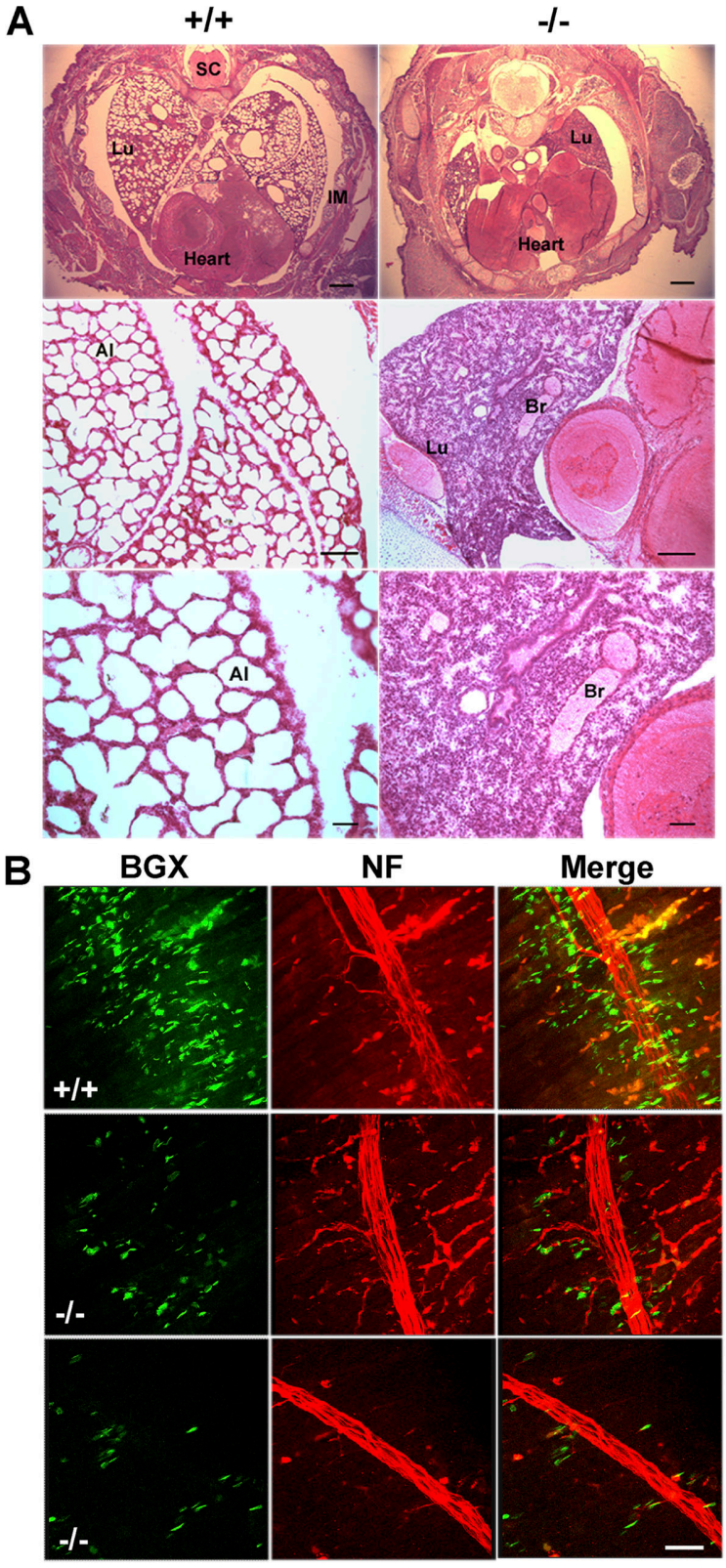

Figure 2. ***Cbx1*$^{-/-}$ neonates do not inflate their lungs, and E19 *Cbx1*$^{-/-}$ embryos exhibit reduced clusters of postsynaptic AChRs within diaphragm muscle.** (A) Hematoxylin and eosin–stained transverse sections through the midbody of wild-type (left) and *Cbx1*$^{-/-}$ (right) neonates showing lack of inflation of the lungs in the *Cbx1*$^{-/-}$ neonates. Al, alveolus; Br, bronchiole; IM, intercostal muscle; Lu, lung; SC, spinal cord. Bars: (top) 450 µm; (middle) 150 µm; (bottom) 50 µm. (B) Staining of E19 wild-type diaphragms (top) with antibodies to NF (red) shows that the diaphragm is clearly innervated. Bungarotoxin-positive (BGX; green) AChRs are clustered around the nerve and its branches. The clusters of bungarotoxin-positive AChRs are much reduced in E19 *Cbx1*$^{-/-}$ diaphragms (middle and bottom), and, in some cases, the branching of the innervating nerve is also reduced (bottom; see red NF staining). Bar, 25 µm.

At E19, the prominent NeuN staining of CP neurons in wild-type brains is absent in CP neurons of *Cbx1*$^{-/-}$ E19 brains (Fig. 3, compare G with H). The amount and heterochromatic localization of Me(3)K9H3 and Me(3)K20H4 were unchanged in *Cbx1*$^{-/-}$ brains (Fig. 3, I–K). Similarly, the amount and distribution of HP1-α and HP1-γ were also unchanged in *Cbx1*$^{-/-}$ brains (Fig. 3 I and Fig. S2, available at http://www.jcb.org/cgi/content/full/jcb.200804041/DC1).

The loss of NeuN staining in postmitotic neurons is thought to be a marker of cell death, where the loss of NeuN staining is

Downloaded from http://rupress.org/jcb/article-pdf/183/4/597/1554702/jcb_200804041.pdf by guest on 09 February 2026

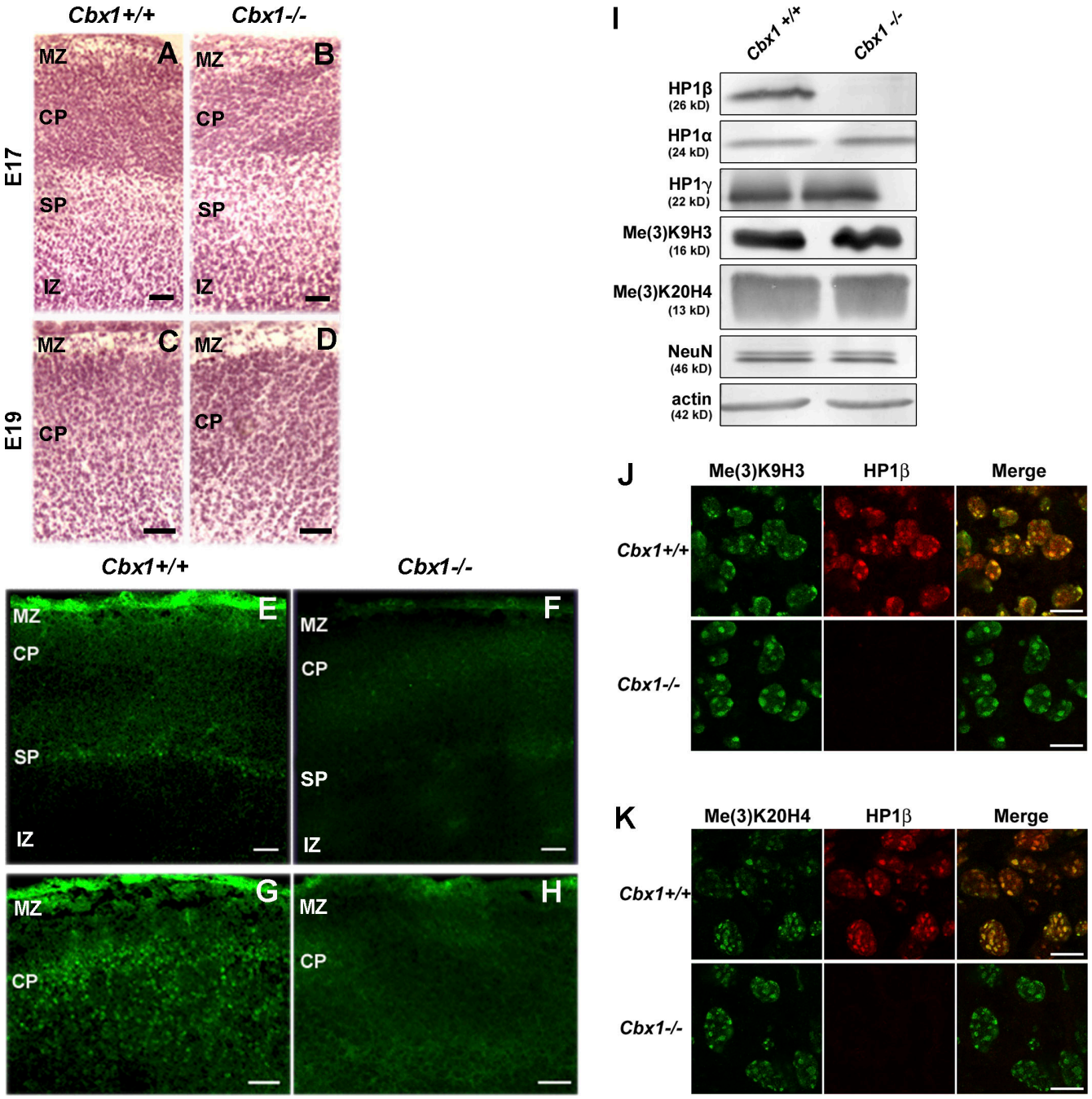

Figure 3. **Immunohistochemical and Western blot analysis of *Cbx1*$^{-/-}$ brains.** (A–D) Hematoxylin and eosin–stained sagittal sections of E17 (A and B) and E19 (C and D) neocortices correspond to the antibody-stained cortices in E–H. Genotypes of the embryos are marked above the photographs. (E–H) α-NeuN–stained E17 and E19 neocortices. The staining of the wild-type E17 cortex with the α-NeuN antibody (E) detects a layer of SP cells that separates the CP from the intermediate zone (IZ). These cells are very weakly stained in the *Cbx1*$^{-/-}$ neocortex (F). Similarly, CP cells are strongly stained with the α-NeuN antibody in the E19 neocortex (G), but such staining of CP cells is reduced to background levels in the E19 *Cbx1*$^{-/-}$ neocortex (H). MZ, marginal zone. (I) HP1-β protein is not detected in extracts from *Cbx1*$^{-/-}$ brains using an antibody to the C terminus of HP1-β; an N-terminal antibody also fails to detect HP1-β in the same way (Fig. S1, available at http://www.jcb.org/cgi/content/full/jcb.200804041/DC1). The levels of HP1-α, HP1-γ, Me(3)K9H3, Me(3)K20H4, and NeuN are not significantly changed in *Cbx1*$^{-/-}$ compared with wild-type brain extracts. The bottom panel is the actin-loading control. Identical results were obtained using whole embryo extracts (not depicted). (J) Me(3)K9H3 heterochromatic distribution is not affected by the *Cbx1*$^{-/-}$ mutation. *Cbx1*$^{-/-}$ and *Cbx1*$^{+/+}$ CP neurons show identical Me(3)K9H3 staining patterns. (K) Me(3)K20H4 heterochromatic distribution is not affected by the *Cbx1*$^{-/-}$ mutation. *Cbx1*$^{-/-}$ and *Cbx1*$^{+/+}$ CP neurons show identical Me(3)K20H4 staining patterns. Bars: (A–H) 100 μm; (J and K) 10 μm.

the result of a loss in antigenicity rather than absolute protein levels (Kuan et al., 2004; Unal-Cevik et al., 2004; Collombet et al., 2006). Therefore, we explored the possibility that the loss of NeuN staining in the *Cbx1*$^{-/-}$ brains might be caused by cell death; Western blot analysis confirmed that NeuN protein levels in *Cbx1*$^{-/-}$ E19 neocortices were the same as in the wild type (Fig. 3 I). We undertook an examination of the integrity of cortical lamination using Nissl staining of semithin sections of neocortex.

Downloaded from http://rupress.org/jcb/article-pdf/183/4/597/1554702/jcb_200804041.pdf by guest on 09 February 2026

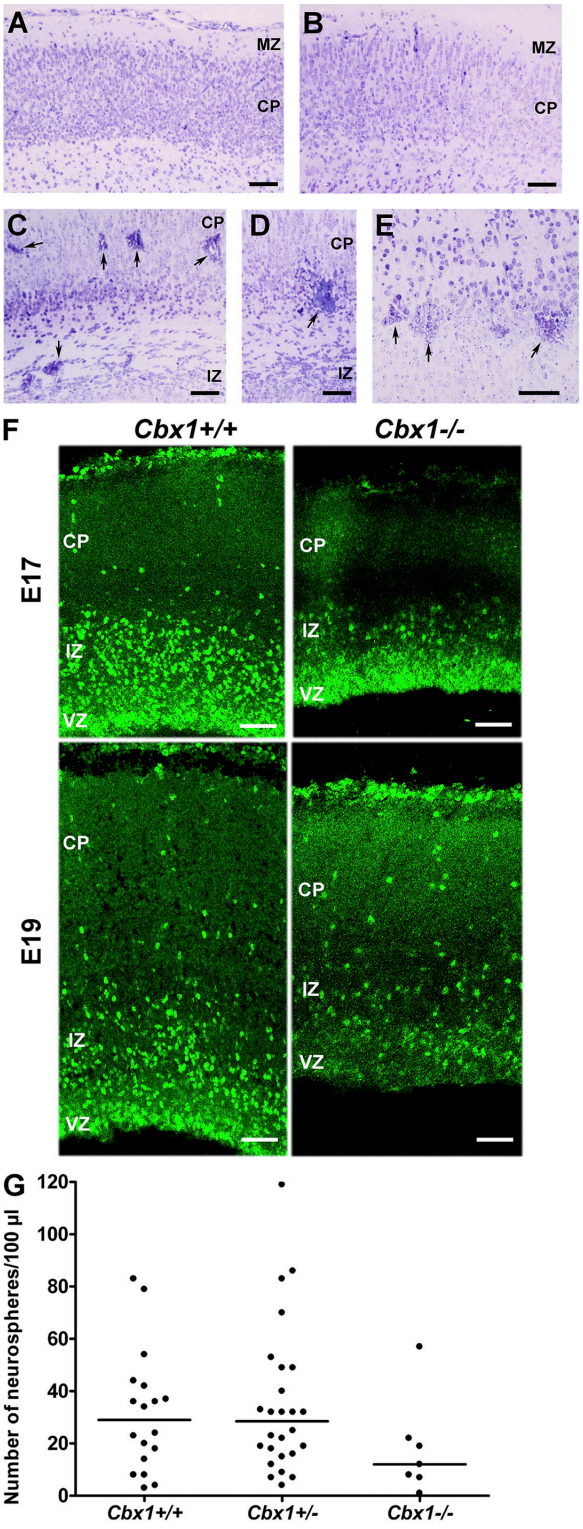

Figure 4. ***Cbx1*$^{-/-}$ mutants exhibit defective cerebral corticogenesis and reduced proliferation of neuronal precursors.** (A and B) Nissl staining of the E19 wild-type neocortex (A) shows the typical ordered arrangement of CP cells. In the E19 *Cbx1*$^{+/-}$ neocortex (B), the ordered arrangement of CP cells is disturbed, and the boundaries at the top and bottom edges of the CP layer are blurred. (C–E) In the E19 *Cbx1*$^{-/-}$ neocortex, the lamination of the neocortex is severely disturbed with patches of edema (C and D, arrows) and clusters of dying cells (E, arrows) scattered through the cortical layers. (F) Proliferating neural progenitors are depleted in the VZ of *Cbx1*$^{-/-}$ brains. On E17, the layer of pKi-67–positive proliferating neural progenitors is thicker in the wild-type VZ compared with the *Cbx1*$^{-/-}$ VZ. On E19, the pool of proliferating progenitors of the *Cbx1*$^{-/-}$ VZ is essentially exhausted compared with the wild-type E19 VZ. (G) There is a trend toward fewer neurospheres from cultures of *Cbx1*$^{-/-}$ brains compared with wild-type and *Cbx1*$^{+/-}$ brains ($P < 0.04$); each dot represents the result from a single embryo. There is no significant difference in the numbers of neurospheres from the wild-type and *Cbx1*$^{+/-}$ brains. Black lines represent the medians. IZ, intermediate zone; MZ, marginal zone. Bars: (A–E) 60 µm; (F) 80 µm.

As shown (Fig. 4 A), control CPs from E19 wild-type neocortices had a normal columnar organization, which was partially disrupted in E19 *Cbx1*$^{+/-}$ brains (Fig. 4 B). In stark contrast, we observed gross changes in the columnar organization in *Cbx1*$^{-/-}$ neocortices (Fig. 4, C–E) that were accompanied by edematous areas (Fig. 4, C and D, arrows) and clusters of dying or dead cells (Fig. 4 E, arrows). These data indicate a strong effect of the *Cbx1*$^{-/-}$ mutation on both cortical lamination and integrity and also show that *Cbx*$^{+/-}$ E19 embryos are haploinsufficient, as they exhibit a partial disruption of laminar organization in the developing neocortex, although *Cbx1*$^{+/-}$ adults are viable and fertile.

It is known that cortical neurons are generated from the proliferating neuronal stem cell precursors located in the ventricular zone (VZ), which lines the lateral cerebral ventricle (Rakic, 1988). Postmitotic neurons migrate away from the VZ and form the distinct cortical layers in an inside-first, outside-last pattern (Desai and McConnell, 2000). We examined cell proliferation in the VZ by staining E17 and E19 wild-type and *Cbx1*$^{-/-}$ brains for the proliferation marker pKi-67. As shown in Fig. 4 F, there is a clear band of pKi-67–positive proliferating cells in the VZ in both the E17 and E19 wild-type brains. This band of pKi-67–positive cells is reduced in E17 *Cbx1*$^{-/-}$ brains and is almost absent in E19 *Cbx1*$^{-/-}$ brains, indicating that the proliferative capacity of the VZ neuronal stem cell pool is reduced in *Cbx1*$^{-/-}$ animals. To gain further insight into the basis of the proliferative defect, we generated neurospheres from wild-type, *Cbx1*$^{+/-}$, and *Cbx1*$^{-/-}$ brains. Accordingly, we dissected E19 brains from the three genotypes and counted the number of neurospheres that develop from the expansion of neural progenitor cells in tissue culture. This showed a trend toward fewer numbers of neurospheres from the *Cbx1*$^{-/-}$ cultures compared with *Cbx1*$^{+/-}$ and wild-type cultures ($P < 0.04$; Fig. 4 G), which is consistent with the E19 pKi-67 staining data (Fig. 4 F). The production of neurospheres from the three genotypes also enabled us to perform a cytogenetic analysis. Examination of *Cbx1*$^{-/-}$ neurospheres showed that there is a statistically significant increase in genomic instability compared with *Cbx1*$^{+/-}$ and wild-type neurospheres as measured by increased premature centromere division (PCD; $P < 0.001$), increased ploidy ($P < 0.001$), micronuclei formation ($P < 0.001$), and, most dramatically, the presence of diplochromosomes (Fig. 5, A–E). *Cbx1*$^{+/-}$ neurosphere cells show a modest increase in chromosomal aberrations when compared with wild type, but its significance is weak (Fig. 5 F and Table S1).

Proliferative defects during the differentiation of neuronal progenitors have been observed in in vitro *Cbx5* (encoding HP1-α) siRNA experiments, in which knockdown of *Cbx5* gene expression results in derepression of E2F-responsive genes and

Downloaded from http://rupress.org/jcb/article-pdf/183/4/597/1554702/jcb_200804041.pdf by guest on 09 February 2026

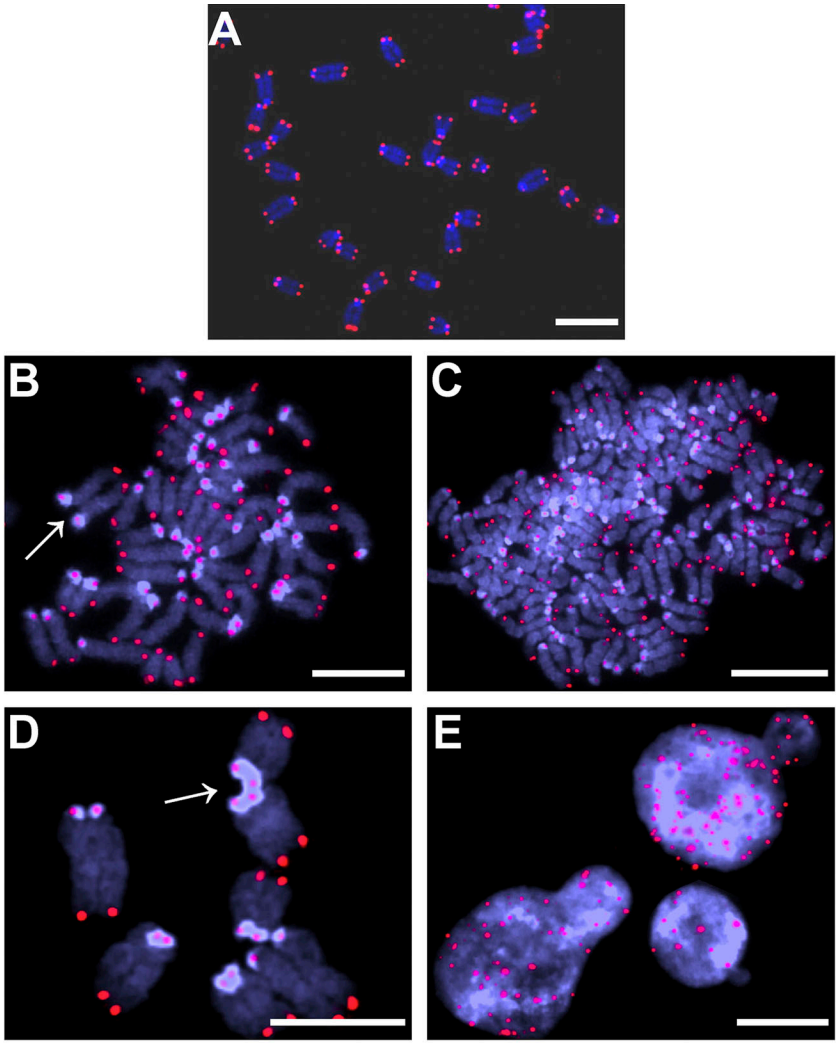

F

	Cbx1+/+	Cbx1+/-	Cbx1-/-
Premature centromere division (PCD)	4%	10%	59%
Increased ploidy	0%	4%	38%
Micronuclei	1%	5%	43%
Diplochromosomes	-	-	+

Figure 5. ***Cbx1*$^{-/-}$ neurospheres exhibit an increased genomic instability.** (A) A mitotic chromosome spread showing the normal situation in which sister chromatids are paired. (B–E) Chromosomes from the *Cbx1*$^{-/-}$ neurosphere cells exhibit a variety of aberrations, including unpaired sister chromatids that have undergone PCD (B, arrow), increased ploidy (C), diplochromosomes (D, arrow), and micronuclei (E). Telomeres (red signals) in all panels were labeled by a specific PNA probe. (F) The table shows that there is a highly significant increase ($P < 0.001$) in PCD, polyploidy, diplochromosomes, and micronuclei between *Cbx1*$^{-/-}$ and the other two genotypes (*Cbx1*$^{+/-}$ and *Cbx1*$^{+/+}$). There is only a borderline significant difference between *Cbx1*$^{+/-}$ and *Cbx1*$^{+/+}$. Bars, 5 µm.

the initiation of abnormal cell cycles that can lead to cell death (Panteleeva et al., 2007). It is unlikely that changes in *Cbx5* gene expression contribute to the *Cbx1*$^{-/-}$ phenotype reported here (Figs. 2–5) because (a) HP1-α protein levels and distribution are not significantly changed in *Cbx1*$^{-/-}$ brain extracts (Fig. 3 I, Fig. S2, and not depicted), and (b) *Cbx5*$^{-/-}$-null mutants are viable and fertile and exhibit no overt neuronal phenotype (not depicted). Rather than the derepression of cell cycle–promoting genes, we suggest that the reduced proliferation and cell death phenotype in *Cbx1*$^{-/-}$ cortices is caused by a severe genomic instability that is the result of an improper constitutive heterochromatin assembly/organization in *Cbx1*$^{-/-}$ cortical neurons. The observed chromosomal aberrations (Fig. 5, A–E) are all consistent with this view. PCD has been observed in the swi6p (fission yeast HP1 homologue) mutant (Nonaka et al., 2001); polyploidy can result from defective kinetochore assembly (Storchová et al., 2006), which requires a platform of HP1-containing heterochromatin (Zhang et al., 2007); undercondensation of centromeric heterochromatin can lead to the exclusion of chromosomes into micronuclei (Guttenbach and Schmid, 1994); and diplochromosomes can result from inefficient deconcatenation of centromeric DNA at the end of mitosis, leading to an extra round of DNA replication without chromatid separation (Sumner, 1998).

It is a matter of speculation as to how the loss of HP1-β could affect the heterochromatin assembly/organization in *Cbx1*$^{-/-}$ cortical neurons. First, it is possible that the loss of HP1-β could result in the misregulation of a critical HP1-β–regulated gene that is required for heterochromatin formation/assembly in neurons; HP1 proteins are known to regulate transcription both positively and negatively (Fanti and Pimpinelli, 2008). Second, it is possible that the defect is structural. According to a current model, the HP1-β–Me(3)K9H3 interaction is weakened by S10-H3 phosphorylation at metaphase, leading to a release

Downloaded from http://rupress.org/jcb/article-pdf/183/4/597/1554702/jcb_200804041.pdf by guest on 09 February 2026

of much of the Me(3)K9H3-bound HP1-β into the nucleoplasm (Fischle et al., 2005). However, it is possible that an immobile fraction of HP1-β bound to the H3 histone fold (Dialynas et al., 2006) still remains associated with the constitutive heterochromatin, and it is the loss of this immobile fraction that leads to the dramatic genomic instability seen in *Cbx1*$^{-/-}$ cortical neurons. We favor the latter because the *Cbx1*$^{-/-}$ phenotype is more severe than the viable double-null *KMT1A/B* compound mutation in which the dynamic histone tail–HP1 interactions within constitutive heterochromatin are disrupted (Peters et al., 2001; Kourmouli et al., 2004). This possibility is further supported by the observation that the overall Me(3)K9H3 and Me(3)K20H4 levels and distribution are unchanged in *Cbx1*$^{-/-}$ neurons (Fig. 3, I–K), although we cannot exclude the possibility that critical sites might be affected. Future work will be directed toward exploring the role of HP1-β in regulating the heterochromatin structure in developing/migrating neurons during cerebral neocortex development.

Materials and methods

Targeted disruption of the *Cbx1* gene and generation of *Cbx1*$^{-/-}$ mice
The targeting vector was constructed from the XhoI–HindIII genomic fragment of *Cbx1* (for a schematic diagram see Fig. 1 A; http://www.ensembl.org/Mus_musculus/geneview?gene=ENSMUSG00000018666). For ease of construction, the *TK-Neo*^{r} gene was inserted into a unique SmaI site found in exon 4 of the *Cbx1* gene (Fig. 1 A). Exon 4 gives rise to bases 320–413 of the *Cbx1* mRNA (A of AUG given as 1) encoding amino acids 108–137 of HP1-β, which lies adjacent to the C terminus of the CD (Ball et al., 1997). The targeting of *Cbx1* with the construct was detected using a 0.3-kb probe from the HP1-β cDNA (Fig. 1 A, shaded boxes). After the digestion of genomic DNA by BamHI, this probe produces a fragment of 11.6 kb for the wild-type allele and 5.3 kb for the targeted allele (because of the introduction of a BamHI site in the *Neo*^{r} gene). Blastocyst injections for the production of germline chimeras and Southern blotting were performed according to standard protocols (Hogan et al., 1994).

Determination of the effect of *Cbx1* gene dosage on hCD2 variegation
The hCD2-1.3B transgene contains the hCD2 promoter driving an hCD2 minigene and 1.3-kb 3′ flanking sequences with a partial locus control region (LCR); i.e., the LCR includes hCD2 DHS1 and DHS2 but lacks DHS3, a site that is essential for full position-independent LCR function and avoidance of PEV. When integrated into pericentric heterochromatin, the transgene variegates (Festenstein et al., 1999). To avoid background effects, heterozygous *Cbx1*$^{+/-}$ mice were backcrossed onto the CBA mouse strain background (more than nine backcrosses). Because homozygous *Cbx1*$^{-/-}$ mice die around birth, we set up timed matings to obtain homozygous embryos with the hCD2 transgene at days 17–19 of embryonic development. Accordingly, we set up the following cross: mice heterozygous for *Cbx1* and hemizygous for hCD2 (*Cbx1*$^{+/-}$ and hCD2$^+$) were mated with mice heterozygous for *Cbx1* (*Cbx1*$^{+/-}$). Day 17–19 embryos resulting from this cross were genotyped for the *Cbx1* mutation by Southern blot analysis (Fig. 1 B), whereas the presence of the hCD2-1.3B transgene was determined by measuring hCD2 expression using FACS.

We measured hCD2 expression in CD4/CD8 double-positive (DP) embryonic thymocytes. Single-cell suspensions were prepared from embryonic thymus and stained for FACS analysis. 10^6 embryonic thymocytes were stained with the following antibody combinations: (a) FITC-conjugated anti-hCD2 (BD), allophycocyanin-conjugated anti-mCD4 (BD), and peridinin-chlorophyll protein complex–conjugated anti-mCD8 (BD) or (b) FITC-conjugated anti-hCD2 (BD), phycoerythrin-conjugated anti-mCD4 (BD), and tricolor-conjugated anti-mCD8 (BD). Three-color FACS analysis was performed on a laser instrument (FACS Calibur; BD) and analyzed using CellQuest software (BD). Live cells were then gated in a ferric-sorbitol-citrate/SSC dot blot, and this gate was used to display CD4 and CD8 expression in a dot blot. Gates for the different populations (double negative, CD4 positive, CD4/CD8 DP, and CD8 positive) were set, and hCD2 expression in each population was displayed as a histogram. To obtain the percentage of hCD2-positive cells, marker regions were set. The percentage of hCD2 expression in CD4/CD8 DP cells from each sample was compiled in a table and displayed as a graph sorted in accordance with the genotype of the sample (Fig. 1 D).

Histology
Whole embryos or brains embedded in paraffin blocks were sectioned to 7 µm and mounted on SuperFrost Plus slides (Menzel-Gläser). Hematoxylin and eosin staining were performed according to standard procedure.

Whole mount immunohistochemistry analyses
E19 dissected thigh muscle and diaphragms were fixed in 2% PFA at 4°C overnight, rinsed briefly with PBS, and incubated in 0.1 M glycine/PBS for 1 h followed by permeabilization in 0.5% Triton X-100/PBS. Tissues were blocked in 10% normal goat serum for 2 h and incubated with primary rabbit antibodies against the light chain of NF (1:200; Millipore) in antibody dilute (Dako) overnight at 4°C. After extensive washing, the tissues were incubated with TRITC-conjugated swine anti–rabbit IgG (1:200; Dako) plus 5 ng/µl AlexaFluor-488–conjugated bungarotoxin (Invitrogen) overnight at 4°C. Tissues were then washed four times for 30 min each with 0.5% Triton X-100/PBS, postfixed in 1% PFA, and mounted in mounting medium (Vector Laboratories).

Immunostaining of cryosections of optimal cutting temperature–embedded brains
Optimal cutting temperature–embedded brains were sectioned at 14–16 µm. The brains were then fixed in 4% PFA for 30 min and blocked in 10% normal goat serum. The primary antibodies used were rat α–HP1-β (MAC 353; 1:50; recognizes the C terminus of HP1-β; Wreggett et al., 1994) and mouse α-NeuN (1:200; Millipore); FITC, fluorescein, or TRITC-conjugated secondary antibodies (Dako) were used to visualize the primary antibody staining. For detection of Me(3)K9H3 and Me(3)K20H4, we used the protocol described in Scholzen et al. (2002). Rabbit antibodies (Me[3]K9H3 and Me[3]K20H4) were detected with an AlexaFluor-488–coupled goat anti–rabbit secondary antibody (Invitrogen). The rat α–HP1-β (Wreggett et al., 1994) antibody was detected with an AlexaFluor-546–coupled goat anti–rat secondary antibody (Invitrogen).

Western blotting of mouse brains
Murine embryonic fibroblast (MEF) cell extracts were prepared according to Cowell et al. (2002). E19 wild-type and *Cbx1*$^{-/-}$ brains were lysed in Laemmli buffer. The extracts were analyzed in 12.5 or 7.5% SDS-PAGE, transferred to nitrocellulose, and probed with the antibodies according to standard procedures (Cowell et al., 2002). The antibody to the N terminus of HP1-β was used at a concentration of 1:100 and was a gift from E. Chan (University of Florida Health Science Center, Gainesville, FL).

Nissl staining of E19 brains
Embryos were perfused via the left ventricle of the heart with 1–2 ml of a 9% NaCl solution containing 0.5% heparin and 0.0266% $NaNO_2$. Subsequently, 20 ml of a 0.1-M Na-cacodylate buffer, pH 7.3, 4% PFA, 2.5% glutaraldehyde, and 1% saccharose were perfused. Heads were postfixed in the same fixative for 3 h at room temperature, and brains were removed, stored overnight in freshly prepared fixative at 4°C, and finally transferred to 0.1-M Na-cacodylate buffer containing 15% saccharose for 2 h. Pieces of occipital cortices of both sides were postfixed in 2% OsO_4, dehydrated, and embedded in epoxy resin. The staining of semithin sections was performed according to Richardson (1966). Before perfusion, the yolk sac was removed for DNA extraction and genotyping.

Neurosphere culture and generation of chromosome spreads from neurospheres
Neurosphere cultures from E19 embryo brains and the production of chromosomes from the neurospheres were performed according to Frappart et al. (2005).

Chromosome experiments and detection of telomeres
Detection of telomeres on metaphase chromosomes was obtained by FISH by using a Cy3-labeled telomere sequence-specific peptide nucleic acid (PNA) probe (Sharma et al., 2003). Giemsa-stained chromosomes of metaphase spreads were analyzed for chromosome aberrations (Fig. 5 F). *Cbx1*$^{-/-}$ and wild-type MEFs were generated according to the 3T9 protocol of Kamijo et al. (1997). Unfixed metaphase chromosomes from the MEFs were stained with anti–HP1-β and –HP1-α antibodies according to Wreggett et al. (1994).

Downloaded from http://rupress.org/jcb/article-pdf/183/4/597/1554702/jcb_200804041.pdf by guest on 09 February 2026

Statistical analysis

Embryo weights. Data were collected at two sites, A and B. There were seven litters in mouse house A and four litters in mouse house B. Four embryos were removed from the analysis, three because of uncertainty about the genotyping and one because it had no tail. The sizes of the litters used in the statistical analysis varied between 2 and 10. A linear mixed model incorporating effects for site, genotype, and litter was fitted to the data. Site and genotype were fitted as fixed effects. Litter was fitted as a random effect. Neither the interaction between site and genotype nor the effect of site was found to be statistically significant. The effect of genotype was highly significant ($P < 0.001$). The embryo weights for +/+ and +/− are not significantly different from each other and are so similar that they can be combined for comparison with the mean weight for −/−. The weights for −/− are significantly lower than those for the other two genotypes (using a *t* test for the difference between two means; $P < 0.01$). On average, −/− embryos are lighter than the others by ∼0.13 g.

Variegation of hCD2 expression. Data were obtained on 44 embryos from six litters. The range of the percentage of CD2 cells per embryo is 8.5–72.7% across all three genotypes. The means and standard deviations for the genotypes (ignoring litter effects) are as follows: +/+ mean = 24.3%, SD = 9.6; +/− mean = 32.1%, SD = 11.3; and −/− mean = 50.2%, SD = 14.1. Litter was fitted as a random effect and genotype as a fixed effect in a restricted maximum likelihood model fitted using the Genstat statistical package (Lawes Agricultural Trust). This showed that there is a highly significant difference between −/− and the other two genotypes ($P < 0.001$). The difference between +/+ and +/− is not significant.

Neurospheres. There is a borderline difference between genotypes when all three experiments are fitted separately ($F = 0.10$ on 2 and 46 degrees of freedom [df]). There is no interaction between experiments; i.e., even though the experiments differ in the mean numbers of neurospheres, these differences are consistent across genotypes. Most of the difference between genotypes clearly lies between −/− and the other two (+/+ and +/−). The total variation resulting from genotype is reduced only very slightly by combining +/+ and +/− and comparing them with −/− (variation explained falls from 4.3 on 2 df to 4.1 on 1 df). In this case, the difference between −/− and +/+ and +/− combined is weakly significant ($F = 4.63$ on 1 and 47 df; $P < 0.04$); the trend is that fewer neurospheres are generated from $Cbx1^{-/-}$ brains.

Chromosomal aberrations in neurosphere cells. For PCD, the raw data per 100 cells are 4 for +/+, 10 for +/−, and 59 for −/−. There is a significant difference between −/− and +/+ and +/− combined ($P < 0.001$; χ^2 test = 96 on 1 df). There is a borderline difference between +/+ and +/− because of the low number of incidences ($P = 0.10$; χ^2 test = 2.8 on 1 df). For ploidy, the raw data per 100 cells are 0 for +/+, 4 for +/−, and 38 for −/−. There is a significant difference between −/− and +/+ and +/− combined ($P < 0.001$; χ^2 test = 72 on 1 df). There is a borderline difference between +/+ and +/− because of the low number of incidences ($P = 0.053$; χ^2 test = 4.1 on 1 df). For micronuclei, the raw data per 100 cells are 1 for +/+, 5 for +/−, and 43 for −/−. There is a significant difference between −/− and +/+ and +/− combined ($P < 0.001$; χ^2 test = 37 on 1 df). There is a borderline difference between +/+ and +/− because of the low number of incidences ($P = 0.097$; χ^2 test = 2.75 on 1 df).

AChRs/micrometer of nerve in mutant ($Cbx1^{-/-}$) and wild-type ($Cbx1^{+/+}$) diaphragms and thigh muscle. The number of AChRs/micrometer of nerve for both mutant and wild-type (diaphragm and thigh) muscles is given in Table S1. Using a simple *t* test, there are significantly fewer AChRs/micrometer in mutant muscles compared with wild-type muscles ($P < 0.004$ for mutant diaphragm vs. wild-type diaphragm; $P < 0.001$ for mutant thigh muscle vs. wild-type thigh muscle).

Image acquisition and manipulation

Make and model of microscope. For Fig. 2 A, we used a Leica MZ16 microscope. For Figs. 2 B, 3 (A–H), and 4 (A–F), we used a Leitz DMRXE microscope. For Fig. 3 (J and K), we used a confocal scanning microscope (TCS-SP; Leica). For Fig. 5, we used a motorized microscope (Axioplan 2ie; Carl Zeiss, Inc.).

Type, magnification, and NA of the objective lenses. For Fig. 2 A, we used a PL Fluotar 10× NA 0.30 objective (Leitz). For Figs. 2 B, 3 (A–H, J, and K), and 4 (A–F), a 63× NA 1.32 HCX plan-Apochromat oil immersion objective was used. For Fig. 5, we used Neofluar 63× NA 1.25 and Plan Neofluar 100× NA 1.3 oil immersion objective lenses.

Temperature. All images were captured at room temperature.

Imaging medium. For Figs. 2 (A and B), 3 (A–H), 4 (A–F), and 5, VECTASHIELD mounting medium with DAPI (Vector Laboratories) was used. For Fig. 3 (J and K), samples were mounted in Dabco solution (0.25% 1,4-diazabicyclo[2.2.2]octane [Sigma-Aldrich], 15 mM NaCl, 0.8 mM Na_2HPO_4, and 0.2 mM KH_2PO_4 in 90% [vol/vol] glycerin, pH 8.6).

Fluorochromes. In Figs. 2 B, 3 (E–H), and 4 F, the fluorochromes used were either FITC- or TRITC-conjugated antibodies or AlexaFluor-488–conjugated bungarotoxin. In Fig. 3 (J and K), AlexaFluor-488 (displayed in green) or AlexaFluor-546 (displayed in red) was used. For Fig. 5, the PNA probe was labeled with Cy3, and the chromosomes were counterstained with DAPI.

Camera make and model. For Fig. 2 A, a Progres C14 camera (Jenoptik) was used. For Figs. 2 B, 3 (A–H), and 4 (A–F), a digital camera (C4742-95; Hamamatsu Photonics) was used. For Fig. 5, we used a charge-coupled device camera (C332843E; JAI Corporation) with 756 × 581 pixels, a 2/3–in. sensing area, a pixel size of 11 × 11 µm, and a signal/noise ratio of >55 dB.

Acquisition software. For Fig. 2 A, we used C14 acquisition software (Jenoptik). For Figs. 2 B, 3 (A–H), and 4 (A–F), we used Openlab 3.0.9 software (PerkinElmer). The acquisition software used for Fig. 3 (J and K) was Leica TCSNT software. For Fig. 5, we used in situ imaging system FISH imaging software (MetaSystems).

Subsequent software used for image processing. Quantitation of AChRs was performed using ImageJ version 1.41i (National Institutes of Health). The confocal z series of diaphragms and thigh muscles stained for both NF and bungarotoxin were taken on a confocal laser microscope (SP5; Leica) using a 20× objective. The number of AChR clusters was calculated in 3D z stacks using an ImageJ plug-in 3D Object Counter (Cordelires and Jackson, 2007) after background subtraction. The lengths of the NF-positive nerves on maximum intensity–projected images were calculated by tracing each individual nerve using the ImageJ plug-in Neuron J (Meijering et al., 2004).

For Figs. 2 (A and B), 3 (A–H), and 4 (A–F), the pictures were assembled using Photoshop CS2 version 9.0 (Adobe Systems, Inc.) for Macintosh. For Fig. 3 I, pictures of specific bands of the indicated antibodies have been assembled. For Fig. 3 (J and K), pictures were processed and assembled with ImageJ and Photoshop 6.0. For Fig. 5, composite images were composed using Photoshop 7.0.1, and the input level was adjusted to match the black background.

Online supplemental material

Fig. S1 shows the lack of N- and C-terminal regions of HP1-β in $Cbx1^{-/-}$ brain extracts. Fig. S2 shows the immunolocalization of HP1-α and HP1-γ proteins in $Cbx1^{+/+}$ and $Cbx1^{-/-}$ E19 cortical sections. Table S1 tabulates the number of AChR clusters/micrometer of nerve in diaphragms and thigh muscle taken from E19 $Cbx1^{+/+}$ and $Cbx1^{-/-}$ embryos. Online supplemental material is available at http://www.jcb.org/cgi/content/full/jcb.200804041/DC1.

P.B. Singh is indebted to Professor J. Gerdes for his encouragement and support. We thank Professor S. Georgatos for critical reading of the manuscript and A. Springbett for help with statistical analysis. We thank Professor E. Chan for the generous provision of the rabbit antiserum raised to the N terminus of HP1-β.

P.B. Singh was supported by Biotechnology and Biological Sciences Research Council core strategic grants and Deutsche Forschungsgemeinschaft grant SI 1209/2-1. R. Fundele was supported by grants from the Swedish Research Council (Vetenskapsrådet) and Wallenberg Consortium North. The T.K. Pandita laboratory was supported by National Institutes of Health grants CA10445 and CA123232.

Submitted: 8 April 2008
Accepted: 9 October 2008

References

Ball, L.J., N.V. Murzina, R.W. Broadhurst, A.R. Raine, S.J. Archer, F.J. Stott, A.G. Murzin, P.B. Singh, P.J. Domaille, and E.D. Laue. 1997. Structure of the chromatin binding (chromo) domain from mouse modifier protein 1. *EMBO J.* 16:2473–2481.

Cheutin, T., A.J. McNairn, T. Jenuwein, D.M. Gilbert, P.B. Singh, and T. Misteli. 2003. Maintenance of stable heterochromatin domains by dynamic HP1 binding. *Science.* 299:721–725.

Cheutin, T., S.A. Gorski, K.M. May, P.B. Singh, and T. Misteli. 2004. In vivo dynamics of Swi6 in yeast: evidence for a stochastic model of heterochromatin. *Mol. Cell. Biol.* 24:3157–3167.

Collombet, J.M., C. Masqueliez, E. Four, M.F. Burckhart, D. Bernabé, D. Baubichon, and G. Lallement. 2006. Early reduction of NeuN antigenicity induced by soman poisoning in mice can be used to predict delayed neuronal degeneration in the hippocampus. *Neurosci. Lett.* 398:337–342.

Downloaded from http://rupress.org/jcb/article-pdf/183/4/597/1554702/jcb_200804041.pdf by guest on 09 February 2026

Cordelires, F., and J. Jackson. 2007. 3D Object Counter. National Institutes of Health, Baltimore, MD. http://rsb.info.nih.gov/ij/plugins/track/objects.html (accessed August, 2008).

Cowell, I.G., R. Aucott, S.K. Mahadevaiah, P.S. Burgoyne, N.S. Huskisson, S. Bongiorni, G. Prantera, L. Fanti, S. Pimpinelli, R. Wu, et al. 2002. Heterochromatin, HP1 and methylation at lysine 9 of histone H3 in animals. *Chromosoma.* 111:22–36.

Daujat, S., U. Zeissler, T. Waldmann, N. Happel, and R. Schneider. 2005. HP1 binds specifically to Lys^{26}-methylated histone H1.4, whereas simultaneous Ser^{27} phosphorylation blocks HP1 binding. *J. Biol. Chem.* 280: 38090–38095.

Desai, A.R., and S.K. McConnell. 2000. Progressive restriction in fate potential by neural progenitors during cerebral cortical development. *Development.* 127:2863–2872.

Dialynas, G.K., D. Makatsori, N. Kourmouli, P.A. Theodoropoulos, K. McLean, S. Terjung, P.B. Singh, and S.D. Georgatos. 2006. Methylation-independent binding of histone H3 and cell-cycle-dependent incorporation of HP1beta into heterochromatin. *J. Biol. Chem.* 281:14350–14360.

Dialynas, G.K., S. Terjung, J.P. Brown, R.L. Aucott, B. Baron-Luhr, P.B. Singh, and S.D. Georgatos. 2007. Plasticity of HP1 in mammalian cells. *J. Cell Sci.* 120:3415–3425.

Eissenberg, J.C., T.C. James, D.M. Foster-Hartnett, T. Hartnett, V. Ngan, and S.C. Elgin. 1990. Mutation in a heterochromatin-specific chromosomal protein is associated with suppression of position-effect variegation in *Drosophila melanogaster*. *Proc. Natl. Acad. Sci. USA.* 87:9923–9927.

Fanti, L., and S. Pimpinelli. 2008. HP1: a functionally multifaceted protein. *Curr. Opin. Genet. Dev.* 18:169–174.

Festenstein, R., S. Sharghi-Namini, M. Fox, K. Roderick, M. Tolaini, T. Norton, A. Saveliev, D. Kioussis, and P.B. Singh. 1999. Heterochromatin protein 1 modifies mammalian PEV in a dose- and chromosomal-context-dependent manner. *Nat. Genet.* 23:457–461.

Festenstein, R., S.N. Pagakis, K. Hiragami, D. Lyon, A. Verreault, B. Sekkali, and D. Kioussis. 2003. Modulation of heterochromatin protein 1 dynamics in primary mammalian cells. *Science.* 299:719–721.

Fischle, W., B.S. Tseng, H.L. Dormann, B.M. Ueberheide, B.A. Garcia, J. Shabanowitz, D.F. Hunt, H. Funabiki, and C.D. Allis. 2005. Regulation of HP1-chromatin binding by histone H3 methylation and phosphorylation. *Nature.* 438:1116–1122.

Frappart, P.O., W.M. Tong, I. Demuth, I. Radovanovic, Z. Herceg, A. Aguzzi, M. Digweed, and Z.-Q. Wang. 2005. An essential function for NBS1 in the prevention of ataxia and cerebellar defects. *Nat. Med.* 11:538–544.

Guttenbach, M., and M. Schmid. 1994. Exclusion of specific chromosomes into micronuclei by 5-azacytidine treatment of lymphocyte cultures. *Exp. Cell Res.* 211:127–132.

Hogan, B., F. Constantini, and E. Lacy. 1994. Manipulating the Mouse Embryo: a Laboratory Manual. Second edition. Cold Spring Harbor Laboratory Press, Cold Spring Harbor, NY. 322 pp.

Jones, D.O., I.G. Cowell, and P.B. Singh. 2000. Mammalian chromodomain proteins: their role in genome organisation and expression. *Bioessays.* 22:124–137.

Kamijo, T., F. Zindy, M.F. Roussel, D.E. Quelle, J.R. Downing, R.A. Ashmun, G. Grosveld, and C.J. Sherr. 1997. Tumor suppression at the mouse *INK4a* locus mediated by alternative reading frame product $p19^{ARF}$. *Cell.* 91:649–659.

Kourmouli, N., P. Jeppesen, S. Mahadevhiah, P. Burgoyne, R. Wu, D.M. Gilbert, S. Bongiorni, S. Prantera, L. Fanti, S. Pimpinelli, et al. 2004. Heterochromatin and *tri*-methylated lysine 20 of histone H4 in animals. *J. Cell Sci.* 117:2491–2501.

Kourmouli, N., Y.M. Sun, P.B. Singh, and J.P. Brown. 2005. Epigenetic regulation of mammalian pericentric heterochromatin in vivo by HP1. *Biochem. Biophys. Res. Commun.* 337:901–907.

Kuan, C.Y., A.J. Schloemer, A. Lu, K.A. Burns, W.L. Weng, M.T. Williams, K.I. Strauss, C.V. Vorhees, R.A. Flavell, R.J. Davis, et al. 2004. Hypoxia-ischemia induces DNA synthesis without cell proliferation in dying neurons in adult rodent brain. *J. Neurosci.* 24:10763–10772.

Locke, J., M.A. Kotarski, and K.D. Tartof. 1988. Dosage-dependent modifiers of position effect variegation in *Drosophila* and a mass action model that explains their effect. *Genetics.* 120:181–198.

Meijering, E., M. Jacob, J.C. Sarria, P. Steiner, H. Hirling, and M. Unser. Design and validation of a tool for neurite tracing and analysis in fluorescence microscopy images. 2004. *Cytometry A.* 58:167–176.

Nielsen, A.L., M. Oulad-Abdelghani, J.A. Ortiz, E. Remboutsika, P. Chambon, and R. Losson. 2001. Heterochromatin formation in mammalian cells: interaction between histones and HP1 proteins. *Mol. Cell.* 7:729–739.

Nonaka, N., T. Kitajima, S. Yokobayashi, G. Xiao, M. Yamamoto, S.I. Grewal, and Y. Watanabe. 2001. Recruitment of cohesion to heterochromatic regions by Swi6/HP1 in fission yeast. *Nat. Cell Biol.* 4:89–93.

Panteleeva, I., S. Boutillier, V. See, D.G. Spiller, C. Rouaux, G. Almouzni, D. Bailly, C. Maison, H.C. Lai, J.P. Loeffler, and A.L. Boutillier. 2007. HP1alpha guides neuronal fate by timing E2F-targeted genes silencing during terminal differentiation. *EMBO J.* 26:3616–3628.

Peters, A.H., D. O'Carroll, H. Scherthan, K. Mechtler, S. Sauer, C. Schöfer, K. Weipoltshammer, M. Pagani, M. Lachner, A. Kohlmaier, S. Opravil, M. Doyle, M. Sibilia, and T. Jenuwein. 2001. Loss of the Suv39h histone methyltransferases impairs mammalian heterochromatin and genome stability. *Cell.* 107:323–337.

Rakic, P. 1988. Specification of cerebral cortical areas. *Science.* 241:170–176.

Rea, S., F. Eisenhaber, D. O'Carroll, B.D. Strahl, Z.W. Sun, M. Schmid, S. Opravil, K. Mechtler, C.P. Ponting, C.D. Allis, and T. Jenuwein. 2000. Regulation of chromatin structure by site-specific histone H3 methyltransferases. *Nature.* 406:593–599.

Richardson, K.C. 1966. Electron microscopic identification of autonomic nerve endings. *Nature.* 210:756.

Schmiedeberg, L., G.K. Weisshart, S. Diekmann, F. Meyer, G. Hoerste, and P. Hemmerich. 2004. High- and low-mobility populations of HP1 in heterochromatin of mammalian cells. *Mol. Biol. Cell.* 15:2819–2833.

Scholzen, T., E. Endl, C. Wohlenberg, S. van der Sar, I.G. Cowell, J. Gerdes, and P.B. Singh. 2002. The Ki-67 protein interacts with members of the heterochromatin protein 1 (HP1) family: a potential role in the regulation of higher-order chromatin structure. *J. Pathol.* 196:135–144.

Schotta, G., M. Lachner, K. Sarma, A. Ebert, R. Sengupta, G. Reuter, D. Reinberg, and T. Jenuwein. 2004. A silencing pathway to induce H3-K9 and H4-K20 trimethylation at constitutive heterochromatin. *Genes Dev.* 18:1251–1262.

Sharma, G.G., K.K. Hwang, R.K. Pandita, A. Gupta, S. Dhar, J. Parenteau, M. Agarwal, H.J. Worman, R.J. Wellinger, and T.K. Pandita. 2003. Human heterochromatin protein 1 isoforms $HP1^{HS\alpha}$ and $HP1^{HS\beta}$ interfere with hTERT-telomere interactions and correlate with changes in cell growth and response to ionizing radiation. *Mol. Cell. Biol.* 23:8363–8376.

Storchová, Z., A. Breneman, J. Cande, J. Dunn, K. Burbank, E. O'Toole, and D. Pellman. 2006. Genome-wide genetic analysis of polyploidy in yeast. *Nature.* 443:541–547.

Sumner, A.T. 1998. Induction of diplochromosomes in mammalian cells by inhibitors of topoisomerase II. *Chromosoma.* 107:486–490.

Thiru, A., D. Nietlispach, H.R. Mott, M. Okuwaki, D. Lyon, P.R. Nielsen, M. Hirshberg, A. Verreault, N.V. Murzina, and E.D. Laue. 2004. Structural basis of HP1/PXVXL motif peptide interactions and HP1 localisation to heterochromatin. *EMBO J.* 23:489–499.

Unal-Cevik, I., M. Kilinç, Y. Gürsoy-Ozdemir, G. Gurer, and T. Dalkara. 2004. Loss of NeuN immunoreactivity after cerebral ischemia does not indicate neuronal cell loss: a cautionary note. *Brain Res.* 1015:169–174.

Wreggett, K.A., F. Hill, P.S. James, A. Hutchings, G.W. Butcher, and P.B. Singh. 1994. A mammalian homologue of *Drosophila* heterochromatin protein 1 (HP1) is a component of constitutive heterochromatin. *Cytogenet. Cell Genet.* 66:99–103.

Zhang, R., S.T. Liu, W. Chen, M. Bonner, J. Pehrson, T.J. Yen, and P.D. Adams. 2007. HP1 proteins are essential for a dynamic nuclear response that rescues the function of perturbed heterochromatin in primary human cells. *Mol. Cell. Biol.* 27:949–962.

Downloaded from http://rupress.org/jcb/article-pdf/183/4/597/1554702/jcb_200804041.pdf by guest on 09 February 2026